Structural, morphological and optical properties of Bi NPs obtained by laser ablation and their selective detection of L-cysteine

Ramon Gabriel Teixeira Rosa [a], Celso de Araujo Duarte [a,*], Wido Herwig Schreiner [a], Ney Pereira Mattoso Filho [a], Arandi Ginane Bezerra Jr. [b], Andersson Barison [c], Fernanda Maria Marins Ocampos [c]

[a] Departamento de Física, Universidade Federal do Paraná Centro Politécnico, CP 19044, 81531-990 Curitiba (PR), Brazil
[b] Departamento Acadêmico de Física, Universidade Tecnológica Federal do Paraná, 80230-901 Curitiba (PR), Brazil
[c] Departamento de Química, Universidade Federal do Paraná Centro Politécnico, CP 19081, 81531-990 Curitiba (PR), Brazil

HIGHLIGHTS

- Bi nanoparticles: production by laser ablation, structure and properties.
- Bi nanoparticles colloid: interaction with amino acids.
- Bi nanoparticles colloid and cysteine: study of fuctionalization.
- Bi nanoparticles colloid as cysteine indicator.

GRAPHICAL ABSTRACT

From a to k: increasing of cysteine concentration on a Bi nanoparticle colloid.
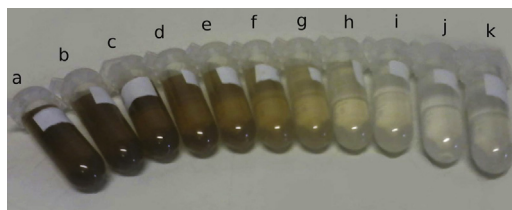
From a to k: increasing of cysteine concentration on a Bi nanoparticle colloid

ARTICLE INFO

ABSTRACT

In the present work we show the results of the investigation of the properties of bismuth nanoparticles (NPs) obtained by the laser ablation in water. The samples were characterized by various techniques: UV/vis spectroscopy, dynamic light scattering, transmission electron microscopy, X-ray photoelectron spectroscopy, X-ray diffraction, nuclear magnetic resonance and zeta potential. The NPs were metallic and surface oxidated, exhibiting absorption peak at 257 nm due to the surface plasmon resonance. The interaction between the NPs and various amino acids was studied and revealed a selective sensibility to cysteine on a range of concentration from 80 to 720 μM, which we attribute to a dimerization of cysteine to cystine probably complexed to the nanoparticle surface by electrostatic interactions, leading to the modification of the NP absorption spectrum.

1. Introduction

Metal and semimetal nanoparticles (NPs) have attracted great attention due to their unique physical properties that are strongly dependent on its size and shape [1,2]. One of the most promising applications is on the area of medical biology. As for example, there is a recent effort on the search for the application of Au NPs as contrasting agent in X-ray imaging [3].

Usually the production of these nanostructures is based on chemical routes that lead to the contamination of the NPs with the chemical reagents [4], which is undesirable for many applications. There are however several alternative ways for the obtainment of such nanoscaled structures. Among them, the laser ablation

* Corresponding author. Tel.: +55 41 33613662; fax: +55 41 33613418.
E-mail addresses: celso@fisica.ufpr.br, celso_ad@hotmail.com
(C. de Araujo Duarte).

technique is particularly convenient due to its simplicity and to the purity of the colloid and the NPs themselves, despite the fact that by chemical routes the control of the NPs constitution and sizes is more effective [4–6].

Au NPs have been actually considered for biomedical applications. For instance, no toxicity was observed in Au-containing NPs for biomedical applications [7,8], and the toxicity of Au is sometimes related to unclean production methods. Another possible candidate for biomedical applications is Bi, due to its low cost and low toxicity [9]. In particular, strictly on the technical aspect, Bi has interesting electrical properties due to a highly anisotropic Fermi surface, such as a small effective electron mass and long Fermi wavelength [10]. These properties lead to fascinating phenomena related to finite-size effects as the semimetal–semiconductor transition in scales of size around 60 nm [10–12]. Despite the formation of NPs during laser ablation involves a convergence of a series of complex phenomena [13], we expect that the low melting point of the Bi will give rise to a high nanoparticles production rate when compared with other metals.

One of the problems on the production of metallic NPs is their coalescence in a broad size distribution [14–16]. However, the size of the coalescences is drastically reduced when the ablation is done in aqueous solution of surfactants, which cover the particles just after their ablation and thus prevent further agglomeration [17–19]. Mafuné et al. [20–22] report the reduction of size distribution for Au, Ag and Pt NPs with sodium dodecyl sulfate (SDS) concentration, resulting in a micelle-water system (two phases).

Recently, Compagnini et al. obtained Au NPs in non-aqueous media by laser ablation in a series of alkanes and alkane–alkanethiol, with control of size and shapes [14,23], providing the stabilization of the colloid and preventing post-ablation agglomeration. The size of the clusters tend to reduce with the increase of thiol concentration. Dodecanethiol-decane solution leads to single crystalline, well separated NPs, while the ablation in pure decane leads to grain boundaries, suggesting a particle agglomeration. The formation of strong dative bonds S-Au limits the particle growth, and the organic alkyl shell prevents agglomeration and stabilizes the colloid.

A very significant effect that emerges on the context of metallic NPs is the surface-enhanced Raman scattering (SERS) [24], which is characterized by the enhancement of the Raman scattering cross-section by a factor up to 10^{14} when Raman-active molecules are adsorbed on the surface of metallic nanostructures with plasmonic properties. SERS originates from the enhancement of the local electromagnetic and from charge-transfer processes between the molecule and the metal substrate. The large intensity of SERS signals enables exploit them in labeling. SERS labels have been used for bioanalytical applications or in vitro/in vivo imaging, like isolated or aggregated gold and silver nanostructures, also with potential for photothermal therapy in the near-infrared spectral window. Recently Amendola and Meneghetti [24] studied the differential Raman scattering cross-section (DRS) of SERS labels based on noble-metal nanoparticles loaded with Raman-active molecules. They verified that proper choice of the Raman reporter and nanoparticle size can enhance the DRS by several orders of magnitude.

On the present work a series of Bi NPs were produced in colloidal form by the laser ablation technique of Bi targets in water medium, and their structural and optical properties were studied. The interaction of the Bi NPs with seventeen different amino acids was studied with the aim of to verify a possible interaction owing to either chemical or biomedical applications.

This work is organized as follows. In Section 2, the details of the experimental setups are described. Section 3 presents the results and the discussions. Finally, the final section contains the conclusions of the work.

2. Experimental

Bi NPs were produced by laser ablation of 99.999% purity Bi pellets produced by Sigma–Aldrich, with the fundamental harmonic of a Nd:YAG laser (1064 nm) operating at 1.5 kHz with 1.0 mJ pulses of 200 ns. The ablation was performed on pellets immersed on bidistilled water (4.0 mL) on a Petri dish. The average distance from the top surface of the targets to the surface of the water was around 2 mm and the laser beam was focused on the surface of the target with a 50 mm convergent lens. The total ablation time was set to exactly 2 min, and the arbitrary choice of this time relies on the practical observation that this was sufficient to give dark brown color to the resulting colloid and that further ablation seemed not to modify substantially the characteristics of the colloid.

The Bi NPs were characterized by UV–visible-NIR absorption spectroscopy, dynamic light scattering (DLS), X-ray diffraction (XRD), transmission electron microscopy (TEM), selected area electron diffraction (SAED), X-ray photoelectron spectroscopy (XPS), nuclear magnetic resonance (NMR) and zeta potential.

UV–vis spectra were obtained with an Ocean-Optics USB 2000+ from 200 nm to 1000 nm with resolution of 2 nm. DLS measurements were done with a Microtrac Nanotrac Ultra. XRD diffractograms were obtained on the Bragg-Brentano $\theta - 2\theta$ geometry with a Shimadzu XRD-7000 diffractometer with the Cu K_{α} line. The samples were prepared through the centrifugation during 8 min at 9000 rpm of 9.0 mL of the colloid equally distributed on six eppendorfs. Approximately 20 μL of the colloid was extracted from the bottom of each recipient and deposited on a glass substrate for immediate measurements with the sample still wet. The TEM and the SAED images were collected with a JEOL JEM 1200EX-II electron microscope, operating with a W filament with accelerating tension of 120 kV. The preparation of samples for TEM and SAED consisted on the dilution of the colloids in water at 1:10 volume ratio, sequentially deposited with a micropipette (20 μL) on carbon coated Cu grid sample holders. For XPS measurements it was added a solution of SDS (sodium dodecyl sulphate) to the colloid in order to stabilize the solution avoiding the formation of NPs aggregates during the drying process. XPS measurements were performed using a VG Microtech ESCA3000 spectometer. The zeta potential measurements were performed with a NanoBrook Zeta-PALS. NMR experiments were acquired at 303 K in H_2O containing drops of D_2O on a Bruker AVANCE III HD 600 NMR spectrometer operating at 14.1 T, observing ^1H and ^{13}C at 600.13 and 150.90 MHz, respectively. The spectrometer was equipped with 5-mm quadrinuclear inverse detection probe with z-gradient. The ^1H spectra was acquired on a spectral width of ∼ 11 ppm, while one-bond (HSQC) and long-range (HMBC) $^1H–^{13}C$ NMR correlation experiments were optimized for average coupling constants $^1J_{(H,C)}$ and $^{LR}J_{(H,C)}$ of 140 and 8 Hz, respectively. All ^1H and ^{13}C NMR chemical shifts were observed in ppm related to TMSP-d_4 signal at 0.00 ppm as internal reference.

3. Results and discussion

3.1. Bi NPs in pure water

First of all, we will present the results of the investigation of Bi NPs on water. In sequence, we will present the analysis of the interaction of the NPs with the different amino acids.

The most immediate characteristic of the samples is their low stability. The dark brown color gives place apparently to a transparent medium with floculated structures within about two days. Owing to this fact we studied the stabilization of the colloid adding 1 mg/mL of SDS, a procedure that was especially convenient on the sample preparation for XPS measurements.
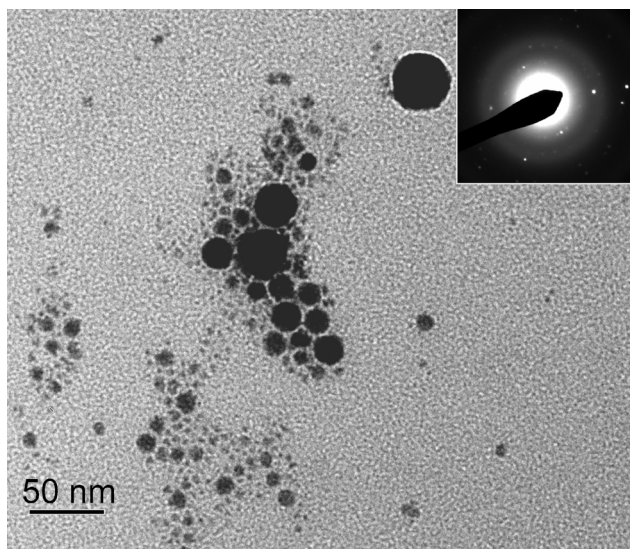
Fig. 1. TEM image of the Bi NPs. The inset shows the SAED pattern of the sample.

In Fig. 1 it is presented the TEM image of Bi NPs on a magnification scale of 40,000×. The inset shows the SAED diffraction pattern. The inspection of the TEM image reveals that the NPs are approximately spherical with a large dispersion on the size distribution, and from the analysis of the SAED pattern we inspect that the NPs are constituted of Bi in metallic form.

The DLS measurements reveals, as can be seen on the plot of Fig. 2, a slightly asymmetric distribution with an average size around 70 nm, and a dispersion in size of a 80 nm FWHM.

The XRD diffractogram is shown in Fig. 3. It can be clearly seen three narrow peaks that are characteristic of metallic Bi, revealing a degree of crystallinity and apparently the absence of oxidized phases. The overall diffractogram also presents a wide peak centered on about 25 degrees and a FWHM of about 10 degrees, attributed to the scattering by the water and the glass substrate.

Fig. 4 presents the absorption spectrum of the colloid on the UV–vis-NIR region. The spectrum is characterized by a single peak at 257 nm with a broad band extended up to around 1000 nm. The 257 nm peak is associated to the surface plasmon resonance, as encountered on the literature [25,26]. Starting at about 950 nm it can be seen an accentuated decrease of the absorption, which points to the existence of a wide peak, which was attributed to the metal–semiconductor transition [25].
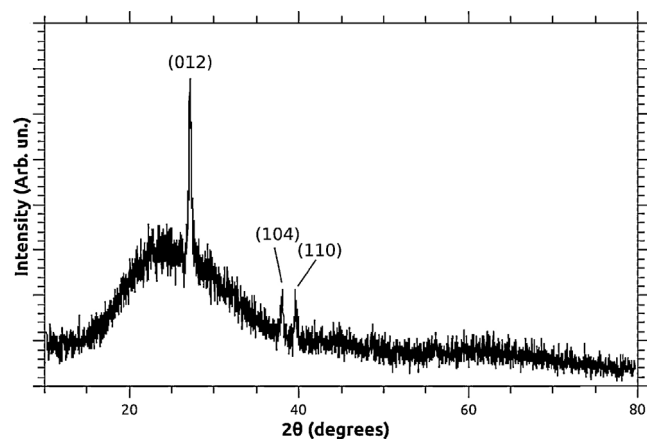

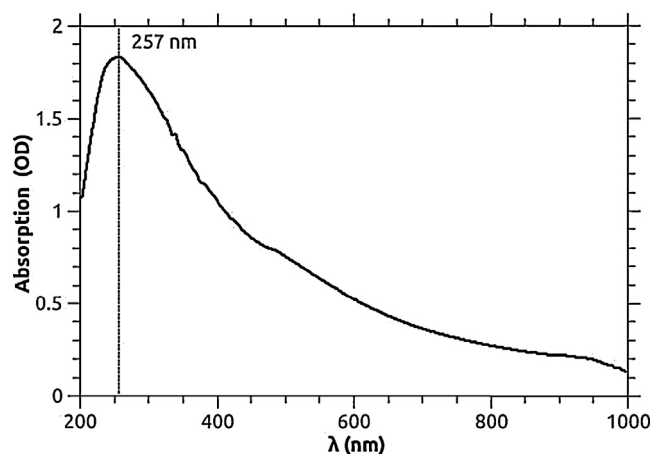**Fig. 3.** XRD diffractogram of the Bi NPs.

Fig. 4. UV–visible–near infrared absorption spectrum of NPs in water colloid.

In Fig. 5 it is presented the XPS spectrum. The analysis of this spectrum reveals that the Bi NPs are actually surface oxidized, a fact that could not be verified on XRD and SAED measurements which were not sufficiently sensitive to give such information. The presence of the oxidized phase Bi_2O_3 is pointed by the appearance of a peak at 158.9 eV, as is well-known in the literature [27].
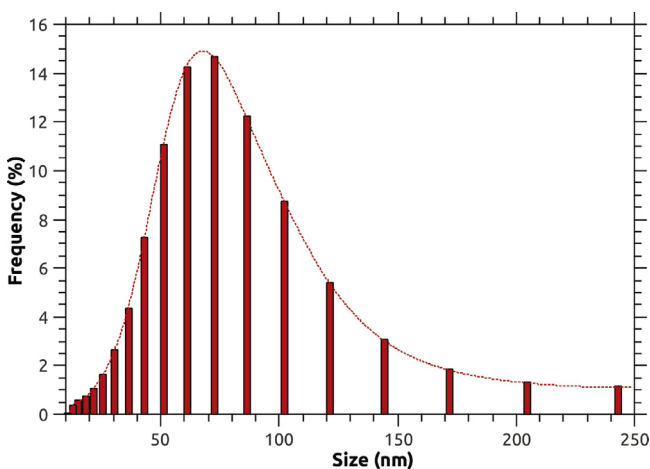

Fig. 2. Size distribution of the Bi NPs obtained by DLS measurements.
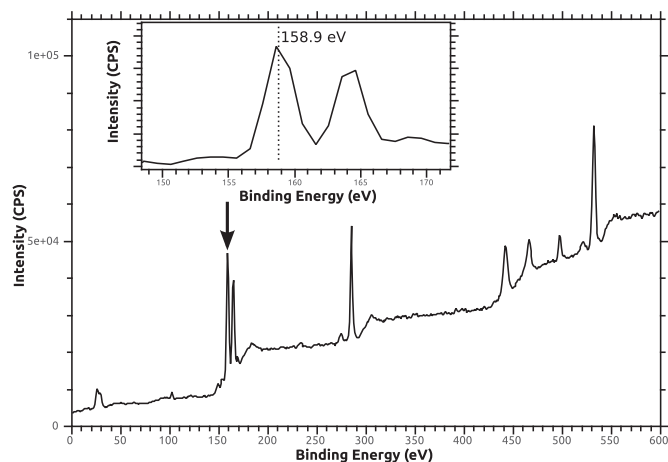

Fig. 5. XPS spectrum of the Bi NPs in water colloid.

Fig. 6. Photograph of a series of eppendorfs with Bi NPs in water with 3.5 mM of different amino acids. From the left to the right: (a) pure colloid; (b) leucine; (c) valine; (d) tyrosine; (e) phenylalanine; (f) histidine; (g) glycine; (h)isoleucine; (i) aspartic acid; (j) metionine; (k) threonine; (l) serine; (m) glutamic acid; (n) arginine; (o) asparagine; (p) glutamine; (q) proline and (r) cysteine.
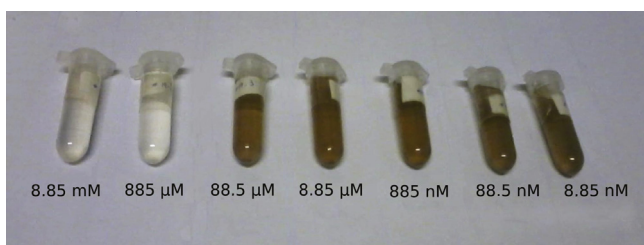

Fig. 7. Photograph of a series of eppendorfs with Bi NPs in water with different concentrations of cysteine.

3.2. Bi NPs in water with different amino acids

In Fig. 6 it is shown a photograph of a series of different samples with the same concentration of Bi NPs with the addition of 5.0 mM of seventeen different amino acids: leucine, valine, tyrosine, phenylalanine, histidine, glycine, isoleucine, aspartic acid, metionine, threonine, serine, glutamic acid, arginine, asparagine, glutamine, proline and cysteine. The addition of any of these amino acids preserve the original color of the produced colloid, except for the case of cysteine, which changed the appearance to transparent in a few seconds. Another feature of the sample with cysteine was its remarkable stability, preserved by undetermined time.[1] On the other side, all the other samples including the pure colloid loose their characteristics about the same period of two days. This points to the fact that cysteine has an important role on the stabilization of the colloid, probably due to a kind of chemical interaction between the amino acid and the NPs.

In Fig. 7 it is presented the photograph of a series of samples as a function of the concentration of cysteine. The inspection reveals immediately the abrupt change of appearance of the colloid for concentrations above 88.5 μM to the transparent solution yet visible at 885 μM. In order to verify more exactly the onset of the transition of physical appearance, we repeated the process studying the phenomenon on this range of concentrations and the result is presented on the photograph of Fig. 8. On this figure it can be seen a gradual transition of appearance.

Fig. 9 shows a series of absorption spectra for the samples shown in Fig. 8 and the spectrum of pure cysteine. The characteristic broad absorption spectrum of the pure colloid yet presented in Fig. 4 suffers a gradual decrease of intensity on its high wavelength region
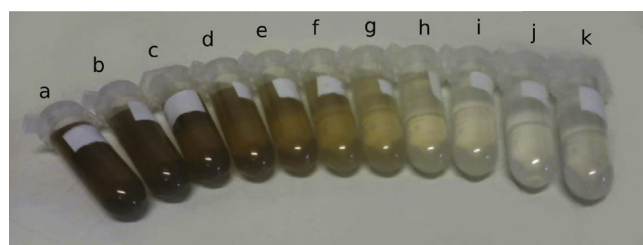
---

[1] Samples of Bi NPs with cysteine produced half a year ago yet preserve the same appearance.

Fig. 8. Photograph of a series of eppendorfs with Bi NPs in water with concentrations of cysteine varying from 80 μM to 800 μM: (a) pure colloid; (b) 80 μM; (c) 160 μM; (d) 240 μM; (e) 320 μM; (f) 400 μM; (g) 480 μM; (h) 560 μM; (i) 640 μM; (j) 720 μM and (k) 800 μM.
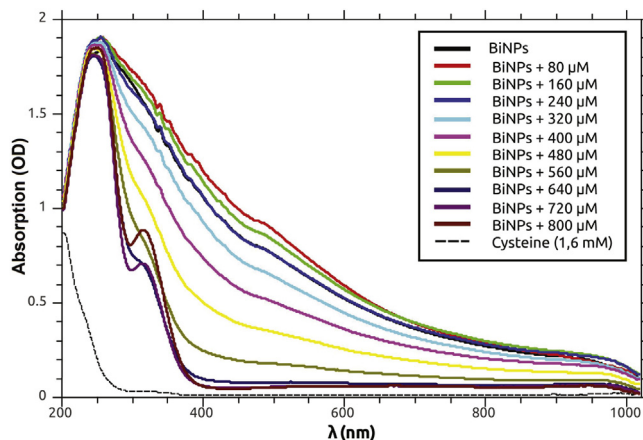

Fig. 9. UV–visible–near infrared absorption spectrum of Bi NPs in solution with different concentration of cysteine.

with the increase of the cysteine concentration, up to a final state (at about the concentration of ~700 μM) when the spectrum is characterized by a pair of peaks. Note that the signal of the surface plasmon remains unaltered. The remarkable dropping of the high wavelength band is further explored in Fig. 10. This figure was obtained from Fig. 9 from the single traces of the absorption as a function of the cysteine concentration for fixed values of the wavelength. This figure shows clearly that in the studied range of wavelengths the variation of the total absorption is almost insensitive to the cysteine concentration for either high or low wavelengths, while on the intermediary region the change in absorption shows typically a monotonic decreasing behavior. This remarkable characteristic reveals that the colloid can be used as an efficient chemical indicator of this amino acid, owing especially to the fact that a calibration process can be suitably applied on the regions of wavelength where
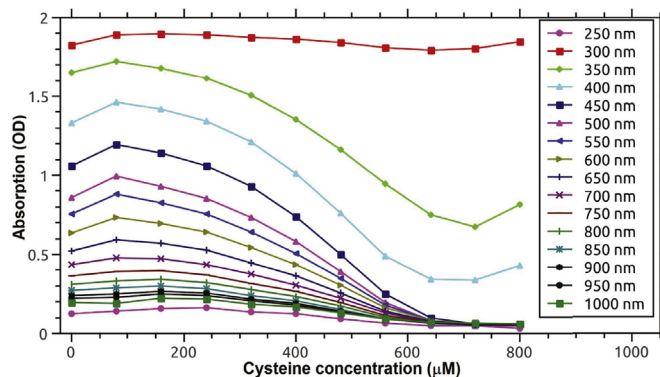

Fig. 10. Optical absorption of the Bi NPs in function of the cysteine concentration at various wavelengths.

Fig. 11. ^{1}H NMR spectra (4.1–2.8 ppm) showing the conversion of cysteine to cystine catalyzed by Bi NPs.

Fig. 12. TEM image of the Bi NPs with addition of cysteine. The inset shows the SAED pattern of the sample.

Table 1
Zeta potential of the Bi NPs with various cysteine concentrations.

Cysteine concentration (μM)	Zeta potential (mV)
0	39.37 ± 0.70
2.6	13.56 ± 1.13
22	-16.35 ± 1.78

an approximate linear behavior (or a low degree polynomial) can be interpolated.

In order to understand the chemical underlying mechanism involving the interaction between Bi NPs and cysteine, a series of ^{1}H NMR measurements has been performed, by adding increasing amounts of cysteine to a solution containing Bi NPs (Fig. 11). The NMR analysis revealed that the Bi NPs has the ability to readily oxide cysteine to cystine, until the system saturation. This found is supported by cystine signals emerging in the ^{1}H NMR spectra (Fig. 11), replacing those of cysteine [28]. After this, the excess of cysteine remains unreacted, although with different NMR chemical shift as those in pure cysteine, probably due to the new environment (Fig. 11). The presence of unreacted cysteine was supported by one-bond and long-range ^{1}H–^{13}C correlation from HSQC and HMBC NMR experiments, which showed identical ^{13}C NMR chemical shift to those of cysteine described in the literature. In the same way, the ^{1}H–^{13}C NMR correlation experiments permitted to obtain the cystine ^{13}C NMR chemical shifts, which were identical to those described in the literature [28]. This is a natural process that, in this case, is catalyzed by Bi NPs. The chemical process of dimerization of cysteine involves the loss of two sulfanyl protons and two electrons, forming a disulfide bond between two cysteine molecules.

Fig. 12 shows the TEM images with 80 $k\times$ magnification and the SAED pattern (inset) of the samples of Bi NPs with addition of cysteine. During the realization of the TEM, we noted that these NPs, unlikely those in pure water, were located only around the metallic regions of the sample holder and believe that this was caused by accumulation of electrostatic charge resultant of the interaction with the cystine. A careful analysis of this image reveals that some nanoparticles show a more irregular shape with a slightly lighter outline. We attribute this subtle fact to the possible complexation of cystine via electrostatic interaction around the NPs. The SAED pattern shows spots related with the metallic Bi. This result is similar to the obtained with the samples in pure water and this reveals that the NPs structure remains unchanged.
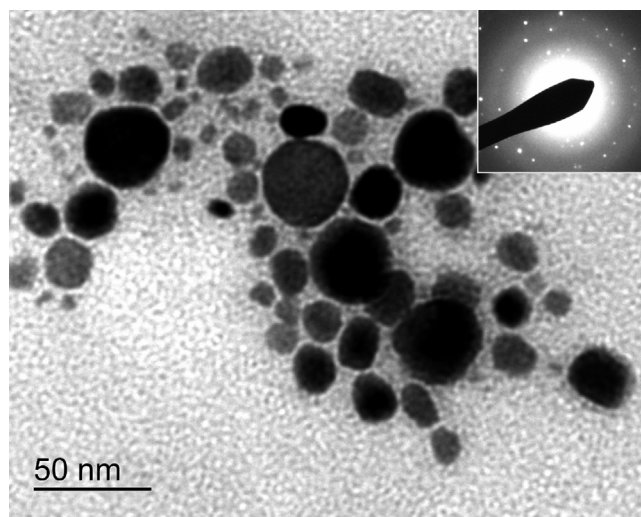
To investigate the process of electrostatic charging of the nanoparticles surface, we performed zeta potential measurements. These results are shown in Table 1.

As can be seen in Table 1, the zeta potential ζ of the colloid decreases with the increase of the cysteine concentration, and changes the signal between the concentrations 2.6 μM and 22 μM. As is well known, large values of the absolute value of the zeta potential reflects high stability of the colloid. Despite this fact, we stress the remarking fact that the higher absolute value of ζ corresponds to the pure colloid without the addition of cysteine, which is the more unstable solution. We believe that in the present case the reduction of the ζ potential does not reflect the actual stability of the colloid since the dimerization of cysteine on cystine impacts on a change of the bare charge of the NPs, which suffers a gradual change of the signal as the cysteine is added to the colloid.

4. Conclusions

As a conclusion we investigated the properties of Bi NPs produced by the laser ablation technique in water and their affinity with a variety of amino acids. We verified that the stability and the appearance of the colloid is remarkably influenced as cysteine is added.

The change in color of the colloid points to a practical application of the colloid as a selective indicator for cysteine. Our results show that it is possible to determine the concentration at a wide range of concentrations of this amino acid at least on the range from 80 μM to 720 μM through the measurement of the absorption spectrum.

References

[1] M. Li, Z. Wang, R.Q. Zhang, A. Soon, Size and dimension effect on volume plasmon energy of nanomaterials, Solid State Commun. 152 (2012) 1564–1566.

[2] K.K. Lance, E. Coronado, L.L. Zhao, G.C. Schatz, The optical properties of metal nanoparticles: the influence of size, shape, and dielectric environment, J. Phys. Chem. B 107 (2003) 668–677.

[3] J.F. Hainfeld, Gold nanoparticles: a new X-ray contrast agent, Br. J. Radiol. 79 (2006) 248–253.

[4] J.A. Dahl, B.L. Maddux, J.E. Hutchison, Toward greener nanosynthesis, Chem. Rev. 107 (2007) 2228–2269.

[5] V. Amendola, M. Meneghetti, Laser ablation synthesis in solution and size manipulation of noble metal nanoparticles, Phys. Chem. Chem. Phys. 11 (2009) 3805–3821.

[6] H. Zeng, X.-W. Du, S.C. Singh, S.A. Kulinich, S. Yang, J. He, W. Cai, Nanomaterials via laser ablation/irradiation in liquid: a review, Adv. Funct. Mater. 22 (2012) 1333–1353.

[7] V. Amendola, S. Scaramuzza, L. Litti, M. Meneghetti, G. Zuccolotto, A. Rosato, E. Nicolato, P. Marzola, G. Fracasso, C. Anselmi, M. Pinto, M. Colombatti, Magneto-plasmonic Au–Fe alloy nanoparticles designed for multimodal SERS-MRI-CT imaging, Small (2014), http://dx.doi.org/10.1002/smll.201303372.

[8] D. Tiedemann, U. Taylor, C. Rehbock, J. Jakobi, S. Klein, W.A. Kues, S. Barcikowski, D. Rath, Reprotoxicity of gold, silver, and gold–silver alloy nanoparticles on mammalian gametes, Analyst 139 (2014) 931–942.

[9] O. Rabin, J. Manuel Perez, J. Grimm, G. Wojtkiewicz, R. Weissleder, An X-ray computed tomography imaging agent based on long-circulating bismuth sulphide nanoparticles, Nat. Mater. 5 (2006) 118–122.

[10] V.S. del'man, Electrons in bismuth, Adv. Phys. 25 (1976) 555–613.

[11] L. Konopko, T.E. Huber, A. Nikolaeva, Quantum interference in bismuth nanowires: evidence for surface charges, J. Low Temp. Phys. 162 (2011) 524–528.

[12] Y. Tian, C. Fei Guo, S. Guo, Y. Wang, J. Miao, Q. Wang, Q. Liu, Bismuth nanowire growth under low deposition rate and its ohmic contact free of interface damage, AIP Adv. 2 (2012), 012112.

[13] Y. Zijie, D.B. Chrisey, Pulsed laser ablation in liquid for micro-/nanostructure generation, J. Photochem. Photobiol. C: Photochem. Rev. 13 (2012) 204–223.

[14] G. Compagnini, A.A. Scalisi, O. Puglisi, C. Spinella, Synthesis of gold colloids by laser ablation in thiol-alkane solutions, J. Mater. Res. 19 (2004) 2795–2798.

[15] A.V. Simakin, V.V. Voronov, G.A. Shafeev, R. Brayner, F. Bozon-Verduraz, Nanodisks of Au and Ag produced by laser ablation in liquid environment, Chem. Phys. Lett. 348 (2001) 182–186.

[16] A.V. Kabashin, M. Meunier, Synthesis of colloidal nanoparticles during femtosecond laser ablation of gold in water, J. Appl. Phys. 94 (2003) 7941–7943.

[17] F. Mafuné, T. Kondow, Formation of small gold clusters in solution by laser excitation of interband transition, Chem. Phys. Lett. 372 (2003) 199–204.

[18] F. Mafuné, J. Kohno, Y. Takeda, T. Kondow, Formation of stable platinum nanoparticles by laser ablation in water, J. Phys. Chem. B 107 (2003) 4218–4223.

[19] F. Mafuné, J. Kohno, Y. Takeda, T. Kondow, Dissociation and aggregation of gold nanoparticles under laser irradiation, J. Phys. Chem. B 105 (2001) 9050–9056.

[20] F. Mafuné, J. Kohno, Y. Takeda, T. Kondow, H. Sawabe, Formation and size control of silver nanoparticles by laser ablation in aqueous solution, J. Phys. Chem. B 104 (2000) 9111–9117.

[21] F. Mafuné, J. Kohno, Y. Takeda, T. Kondow, H. Sawabe, Structure and stability of silver nanoparticles in aqueous solution produced by laser ablation, J. Phys. Chem. B 104 (2000) 8333–8337.

[22] F. Mafuné, J. Kohno, Y. Takeda, T. Kondow, H. Sawabe, Formation of gold nanoparticles by laser ablation in aqueous solution of surfactant, J. Phys. Chem. B 105 (2001) 5114–5120.

[23] G. Compagnini, A.A. Scalisi, O. Puglisi, Production of gold nanoparticles by laser ablation in liquid alkanes, J. Appl. Phys. 94 (2003) 7874–7877.

[24] V. Amendola, M. Meneghetti, Exploring how to increase the brightness of surface-enhanced Raman spectroscopy nanolabels: the effect of the Raman-active molecules and of the label size, Adv. Funct. Mater. 22 (2012) 353–360.

[25] R.K. Verma, K. Kumar, S.B. Rai, Near infrared induced optical heating in laser ablated Bi quantum dots, J. Coll. Interface Sci. 390 (2013) 11–16.

[26] Y.W. Wang, B.H. Hong, K.S. Kim, Size control of semimetal bismuth nanoparticles and the UV–visible and IR absorption spectra, J. Phys. Chem. B 109 (2005) 7067–7072.

[27] J.F. Moulder, W.F. Stickle, P.E. Sobol, K.D. Bomben, Handbook of X ray photoelectron spectroscopy: a reference book of standard spectra for identification and interpretation of Xps data, Phys. Electron. (1995), ISBN 096481241X.

[28] D.S. Wishart, C.G. Bigam, A. Holm, R.S. Hodges, B.D. Sykes, 1H, 13C and 15N random coil NMR chemical shifts of the common aminoacids. I. Investigations of nearest-neighbor effects, J. Biomol. NMR 5 (1995) 67–81.